# Matrix Infrared Spectroscopic and Computational Investigation of Late Lanthanide Metal Hydride Species MH$_x$(H$_2$)$_y$ (M = Tb−Lu, $x$ = 1−4, $y$ = 0−3)[†]

## Xuefeng Wang,[‡] Lester Andrews,*[,‡] Ivan Infante,[§] and Laura Gagliardi*[,§,‖]

*Department of Chemistry, University of Virginia, Charlottesville, Virginia 22904-4319, Department of Physical Chemistry, University of Geneva, 30 Quai Ernest Ansermet, CH-1211 Geneva, Switzerland, and Department of Chemistry, University of Minnesota and Minnesota Supercomputing Institute, 207 Pleasant Street SE, Minneapolis, Minnesota 55455*

*Received: May 11, 2009; Revised Manuscript Received: June 26, 2009*

Laser-ablated late lanthanide metal atoms were condensed with pure hydrogen at 4 K, and new infrared absorptions are assigned to binary metal hydrides on the basis of deuterium substitution and density functional theory frequency calculations. The dominant absorptions in the 1330−1400 cm$^{-1}$ region are identified as LnH$_3$ complexes with very weak ligand bands near 3900 cm$^{-1}$. With ytterbium, YbH and YbH$_2$ were the major initial products, but YbH$_3$ increased at their expense upon sample irradiation. Evidence is also presented for the LuH and ErH molecules and the tetrahydride anions in solid hydrogen.

## Introduction

Lanthanide metal chemistry is dominated by the III oxidation state, and most of the hydride chemistry involves trihydrides.[1] There is, however, some work with II state compounds[1] and very recently Yb(II) complexes have been compared with calcium analogues.[2] There is considerable interest in the II state LnO diatomics and the I state diatomic LnH molecules, particularly from the theoretical standpoint with respect to the f-orbital core electronic configurations.[3−6] It has been shown, however, that 4f electrons do not participate explicitly in lanthanide metal−ligand bonding.[7] Binary Ln$_n$H$_{3n}$ metal clusters are predicted theoretically to be stable and thus to provide links between small molecules and bulk solid lanthanide hydrides.[8] The latter bulk materials remain of interest for their semiconductor, magnetic, and optical properties.[9−11]

Pure hydrogen has been used as the reagent to prepare new hydrides and the matrix to isolate them at 4 K.[12] This procedure gives a large yield of the binary metal hydride, and extensive dihydrogen complexation can result for favorable cases such as tungsten, ruthenium, and actinide hydrides.[13−15] Our investigation for the early lanthanide metals (Ce−Gd) revealed the trihydride as the dominant species, except for EuH$_2$, and gave dihydrides for these metal reactions in pure hydrogen.[16] Both spectroscopic and computational evidence showed stronger, more extensive dihydrogen complex formation for the dihydride than for the trihydride core molecules. Here we extend this investigation to the late lanthanide metals (Tb−Lu) and again find dominance of the trihydride products. In contrast similar reactions with 2% H$_2$ in argon gave the LnH$_2$ molecules as the dominant product.[17]

## Experimental and Computational Methods

The experimental apparatus and procedure for investigating reactions of laser-ablated lanthanide metal atoms with hydrogen molecules during condensation at 4 K has been described in earlier works.[12,18] The Nd:YAG laser fundamental (1064 nm, 10 Hz repetition rate with 10 ns pulse width) was focused onto a freshly cleaned lanthanide metal target (Johnson-Matthey) freshly mounted on a rotating rod. The laser energy was varied from 1 to 5 mJ/pulse. Laser-ablated lanthanide metal atoms were thus codeposited with 3−4 mmol of normal hydrogen molecules onto a CsI cryogenic window at 4 K for 30 min using a Sumitomo Heavy Industries model RDK-205D refrigerator. Hydrogen (Matheson), D$_2$, and HD (Cambridge Isotopic Laboratories) were used in different experiments. FTIR spectra were recorded at 0.5 cm$^{-1}$ resolution on a Nicolet 750 FTIR instrument with 0.1 cm$^{-1}$ accuracy using a HgCdTe range B detector. Matrix samples were annealed at different temperatures, and selected samples were subjected to broad band photolysis by a medium-pressure mercury arc street lamp (Philips, 175 W) with the outer globe removed.

Quantum chemical calculations were performed for late LnH$_x$ core molecules and LnH$_x$(H$_2$)$_y$ complexes using density functional theory (DFT) in analogy with our previous work on the early lanthanide metals.[16] The TURBOMOLE package was employed.[19] Scalar relativistic effects were incorporated by employing on the lanthanide metal atoms the Stuttgart RSC Segmented/ECP basis set with 28 core electrons and contraction of (14s13p10d8f3g)/[10s8p5d4f3g] type.[5] A valence triple-ζ split valence basis set, TZVPP, was used on the hydrogen atoms. The gradient-corrected BP86 exchange correlation (xc) functional and the PBE0 functional were employed. Full geometry optimizations, frequency calculations, and assessment of the correct ground state spin multiplicity were performed for all species. Basis set superposition error (BSSE) corrections were included using the counterpoise method. Zero point energy corrections (ZPE) were also computed. Some of the calculations were repeated using the complete active space (CAS) SCF method[20] followed by multiconfigurational second-order perturbation theory (CASPT2).[21] Scalar relativistic effects were included using the Douglas−Kroll−Hess Hamiltonian[22] and relativistic ANO-RCC basis set of VTZP quality, as implemented in the MOLCAS 7.2 package.[23] In the CASSCF treatment, the molecular orbitals formed by linear combinations
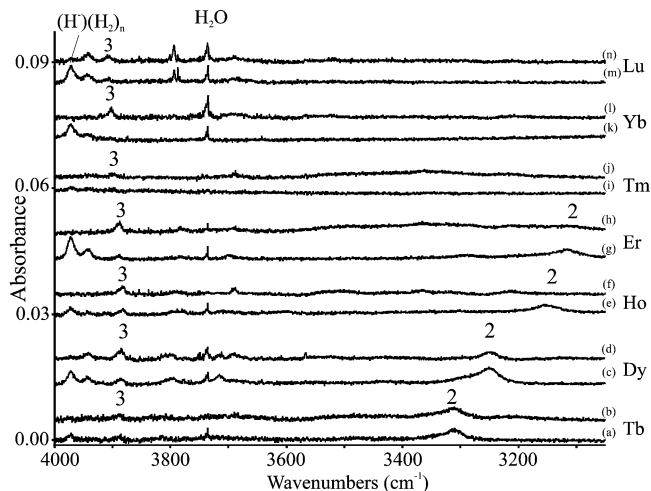
---

**Figure 1.** Infrared spectra for the products of reaction of late lanthanide metal atoms with dihyrogen during co-condensation at 4 K: (a) Tb codeposition, (b) after >290 nm irradiation; (c) Dy codeposition, (d) after >380 nm irradiation; (e) Ho codeposition, (f) after >290 nm irradiation; (g) Er codeposition, (h) after >290 nm irradiation; (i) Tm codeposition, (j) after >380 nm irradiation; (k)Yb codeposition, (l) after >470 nm irradiation; (m) Lu codeposition, (n) after >290 nm irradiation.
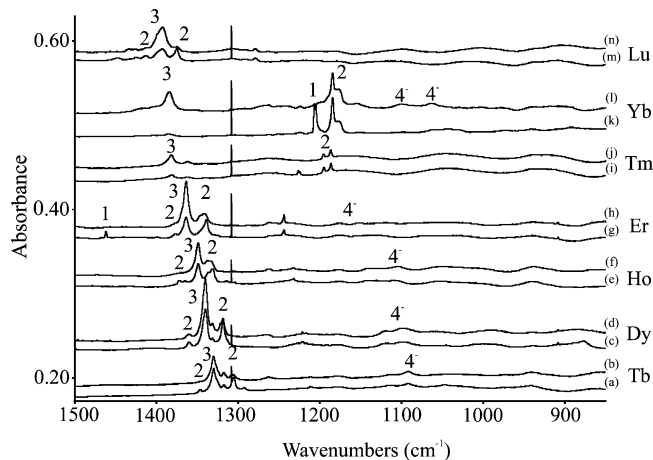


**Figure 2.** Infrared spectra for the products of reaction of late lanthanide metal atoms with dihyrogen during co-condensation at 4 K: (a) Tb codeposition, (b) after >290 nm irradiation; (c) Dy codeposition, (d) after >380 nm irradiation; (e) Ho codeposition, (f) after >290 nm irradiation; (g) Er codeposition, (h) after >290 nm irradiation; (i) Tm codeposition, (j) after >380 nm irradiation; (k)Yb codeposition, (l) after >470 nm irradiation; (m) Lu codeposition, (n) after >290 nm irradiation.
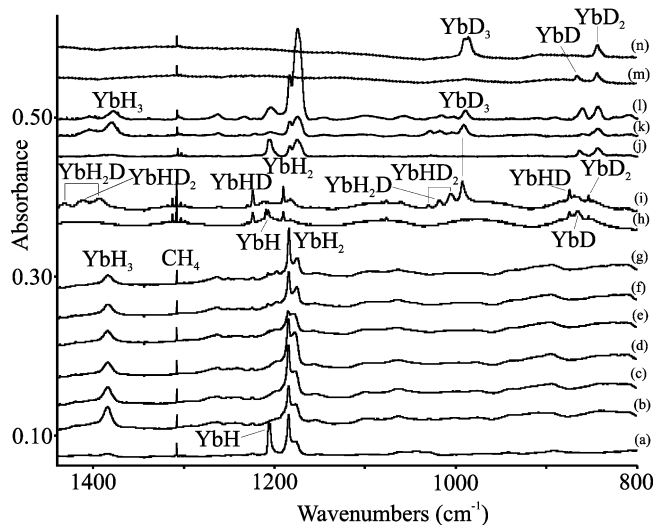
of 6s, 5d, and 4f orbitals of the lanthanide atom with the 1s orbital of the hydrogen atoms were included in the active space. In the subsequent CASPT2 calculations, the [Xe] 4d orbitals of the lanthanide atoms were kept frozen. This approach has been shown to work successfully in a number of earlier applications.[24−30]

## Results and Discussion

Infrared spectra of late lanthanide metal hydride complexes in solid hydrogen and computations to assist in their identification and assignment will be presented. We will first identify the LnH$_x$ core molecules in the LnH$_x$(H$_2$)$_y$ complexes, and then make an attempt to estimate $y$ values from calculations of these complexes as models for the hydride core molecules trapped in the solid hydrogen matrix environment.

**Infrared Spectra.** The infrared spectra for the products of reaction of late lanthanide metal atoms with dihydrogen are reported in Figures 1−6 and in Figure 7 possible binding motifs of lanthanide hydrides with H$_2$ are depicted.

Table 1 summarizes the most important infrared bands. The experimental values are reported together with several calculated ones.

Normal hydrogen was codeposited with laser-ablated late lanthanide metal atoms onto a CsI window maintained at 4 K. The infrared spectra contain bands due to solid hydrogen and the trapped hydride anion (H$^-$)(H$_2$)$_n$ as it perturbs the surrounding dihydrogen ligands.[31] Figures 1 and 2 illustrate infrared spectra in the H−H and Ln−H stretching regions for each late lanthanide metal (Tb−Lu) after codeposition and after irradiation in the visible region and final exposure to 240−380 nm mercury arc light. The strong dominant band (labeled 3 for the trihydride core species) in the Ln−H stretching region (Figure 2) ranges from 1330.1 cm$^{-1}$ for Tb to 1393.9 cm$^{-1}$ for Lu as summarized in Table 1. These bands increase and then decrease during the irradiation sequence in each metal experiment as shown in detail for Yb in Figure 3. The absorptions labeled 3 and their deuterium counterparts for all seven metals reveal three bands with HD for the three unique Ln−H and three more bands for the unique Ln−D stretching modes as shown for YbH$_2$D and



**Figure 3.** Infrared spectra for the major Yb atom reaction products with isotopic molecular hydrogen samples during codeposition at 4 K: (a) H$_2$, (b) after >470 nm irradiation, (c) after >380 nm irradiation, (d) after >290 nm irradiation, (e) after >240 − 380 nm irradiation, (f) after annealing to 6 K, and (g) after annealing to 6.5 K; (h) HD, (i) after >470 nm irradiation, (j) H$_2$ + D$_2$, (k) after >470 nm irradiation, (l) after >290 nm irradiation; (m) D$_2$, (n) after >470 nm irradiation. The labels identify the core isotopic molecules in larger complexes. In the HD experiment the YbH$_2$(D$_2$), YbD$_2$(H$_2$), and YbD$_3$(L) complexes are implicated through isotopic positional exchange.

YbHD$_2$ in Figure 3. The strong 1384.3 cm$^{-1}$ band for the YbH$_3$ core molecule in solid hydrogen shifts to 990.7 cm$^{-1}$ in solid deuterium (H/D isotopic frequency ratio 1.4005), and these give way in solid HD to new bands at 1432.0, 1410.7, and 1393.0 cm$^{-1}$ in the Yb−H stretching region and at 1029.5, 1018.2, 1005.5, and 993.0 cm$^{-1}$ in the Yb−D region. The 1432.0 and 1393.0 cm$^{-1}$ bands are symmetric and antisymmetric Yb−H stretching modes of the YbH$_2$D core, and the 1018.2 cm$^{-1}$ band is the corresponding Yb−D mode, the 1410.7 cm$^{-1}$ peak is the Yb−H, and the 1029.5 and 1005.5 cm$^{-1}$ the Yb−D vibrations of the YbHD$_2$ core. Notice that the latter bands are slightly stronger than the former despite the lower intensity (about half) of the metal−D modes and the presence of an even stronger
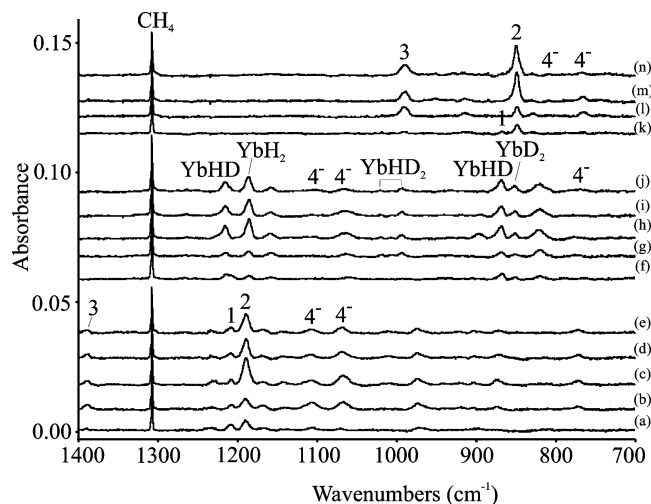
**Figure 4.** Infrared spectra for the major Yb atom reaction products with isotopic molecular hydrogens (4%) in neon during codeposition at 4 K: (a) H₂, (b) after >470 nm irradiation, (c) after >290 nm irradiation, (d) after >220 nm irradiation, and (e) after annealing to 8 K; (f) HD, (g) after >470 nm irradiation, (h) after >290 nm irradiation, (i) after 240−380 nm irradiation, and (j) after annealing to 8 K; (k) D₂, (l) after >470 nm irradiation, (m) after 240−380 nm irradiation, and (n) after annealing to 8 K. The labels identify the core isotopic molecules in larger complexes. In the HD experiment the $YbH_2(D_2)$ and $YbD_2(H_2)$ complexes are implicated through isotopic positional exchange.



**Figure 5.** Infrared spectra for the products of reaction of late lanthanide metal atoms with dideuterium during co-condensation at 4 K: (a) Tb codeposition, (b) after >4700 nm irradiation, (c) after >380 nm irradiation, (d) after 240−380 nm irradiation; (e) Dy codeposition, (f) after >290 nm irradiation; (g) Ho codeposition, (h) after >290 nm irradiation; (i) Er codeposition, (j) after >290 nm irradiation; (k) Tm codeposition, (l) after >530 nm irradiation, (m) after >290 nm irradiation; (n)Yb codeposition, (o) after >470 nm irradiation; (p) Lu codeposition, (q) after >290 nm irradiation.

993.0 cm⁻¹ band, which is thus due to the YbD₃ core molecule in solid HD. In contrast, there is no evidence for the YbH₃ core molecule in solid HD (Figure 3). We are observing the consequence of H/D isotopic exchange between the core (*x*) hydrides and the (*y*) hydrogen ligands during exothermic reactions, which clearly favors D bonded to the metal center rather than H. Such isotopic exchange has been observed for several transition metal complexes prepared with HD.[13,14,32]

Slightly weaker bands labeled 2 (for the dihydride core species) appear just below the corresponding 3 band, save for
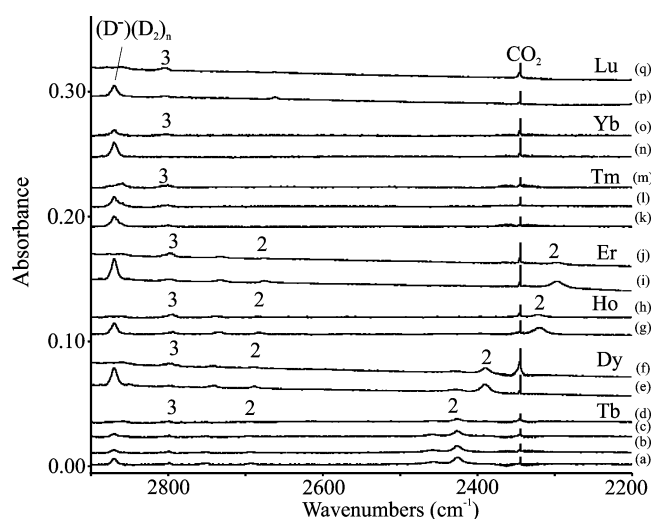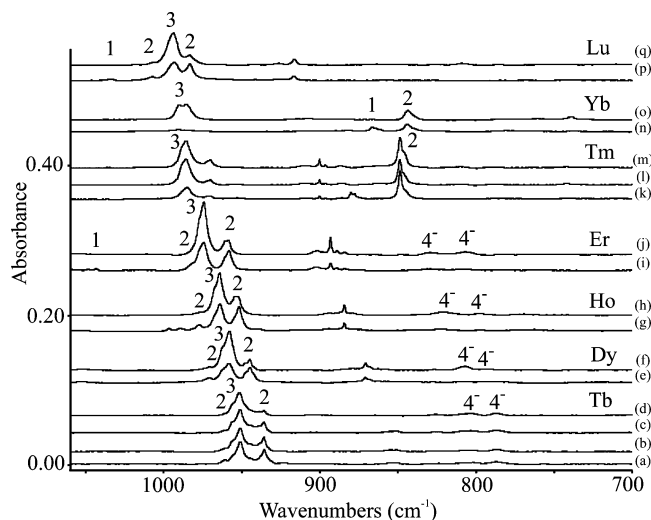


**Figure 6.** Infrared spectra for the products of reaction of late lanthanide metal atoms with dideuterium during co-condensation at 4 K: (a) Tb codeposition, (b) after >4700 nm irradiation, (c) after >380 nm irradiation, (d) after 240−380 nm irradiation; (e) Dy codeposition, (f) after >290 nm irradiation; (g) Ho codeposition, (h) after >290 nm irradiation; (i) Er codeposition, (j) after >290 nm irradiation; (k) Tm codeposition, (l) after >530 nm irradiation, (m) after >290 nm irradiation; (n)Yb codeposition, (o) after >470 nm irradiation; (p) Lu codeposition, (q) after >290 nm irradiation.
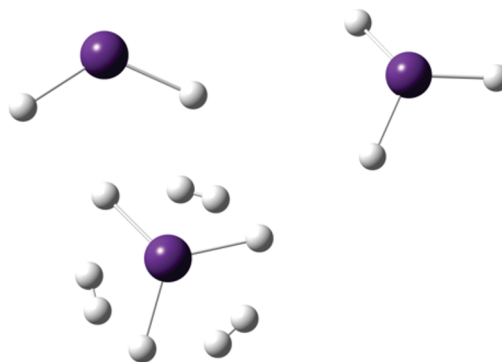


**Figure 7.** Possible binding motifs of lanthanide hydrides with H₂. In this specific case the structures of TbH₂, TbH₃, and TbH₃ with three H₂ molecules are reported.

Tm and Yb where the 2 bands fall 200 cm⁻¹ lower, and a weaker 2 band is higher for Tb, Dy, Ho, and Er (Figure 2). The 2 bands decrease on irradiation when the 3 band increases, but this process is reversed with >380 nm irradiation for the Yb system (Figure 3c). The sharp 1184.5 cm⁻¹ dihydride core band is particularly clear in the Yb and hydrogen system (Figure 3), and it shifts to 844.1 cm⁻¹ in the deuterium sample, defining an H/D ratio of 1.4033. After vis photolysis to eliminate YbH in the solid HD sample (Figure 3h,i), two sharp bands increase at 1190.2 and 1223.7 cm⁻¹. The 1190.2 cm⁻¹ band is assigned to $YbH_2(D_2)(HD)_{y-1}$ where the 5.7 cm⁻¹ blue shift is ascribed to different ligands relative to H₂, and again isotopic exchange has taken place during the exothermic (reaction 1a). The sharp 1223.7 cm⁻¹ band is then due to $YbHD(HD)_y$.

$$Yb + (y + 1)H_2 \rightarrow [YbH_2]^*(H_2)_y \rightarrow YbH_2(H_2)_y$$

(1a)

$$\text{Yb} + (y + 1)\text{HD} \rightarrow [\text{YbHD}]^*(\text{HD})_y \rightarrow \text{YbHD}(\text{HD})_y \quad (1b)$$

$$\text{Yb} + (y + 1)\text{HD} \rightarrow [\text{YbHD}]^*(\text{HD})_y \rightarrow \text{YbH}_2(\text{D}_2)(\text{HD})_{y-1} \quad (1c)$$

$$\text{Yb} + (y + 1)\text{HD} \rightarrow [\text{YbHD}]^*(\text{HD})_y \rightarrow \text{YbD}_2(\text{H}_2)(\text{HD})_{y-1} \quad (1d)$$
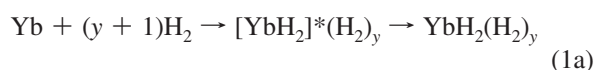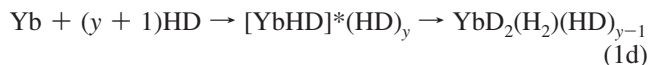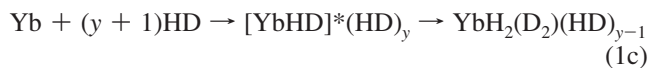
Corresponding spectra are observed in the Yb−D region at 853.3 cm$^{-1}$ for YbD$_2$(H$_2$)(HD)$_{y-1}$ and at 874.1 cm$^{-1}$ for YbHD(HD)$_y$. The 1223.7/874.1 ratio 1.4000 is appropriate for this Yb−H(D) stretching mode assignment. The observation of two stretching bands for the YbHD core molecule thus confirms the dihydride core molecule assignment.

The previous 2% H$_2$/argon matrix experiments with Yb give very different spectra. First, the strong YbH$_2$ band at 1219.3 cm$^{-1}$ doubles on UV irradiation along with its weaker 1277.2 cm$^{-1}$ companion (these antisymmetric and symmetric stretching mode assignments are verified by HD substitution).[17] The 34.8 cm$^{-1}$ shift from 1219.3 to 1184.5 cm$^{-1}$ is thus due to hydrogen ligands and matrix environment. A weak 1431 cm$^{-1}$ band increases on UV irradiation and annealing, and this could be due to YbH$_3$. The shift from solid hydrogen would again be ascribed to the surrounding hydrogen molecules.

The present 4% H$_2$/neon matrix experiments with Yb exhibited behavior more nearly like hydrogen than like argon.

**TABLE 1: Infrared Absorptions (cm$^{-1}$) Observed for Late Lanthanide Metal Atom Reaction Products with Pure Hydrogen or Deuterium at 4 K$^a$**

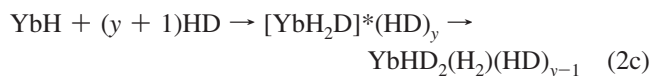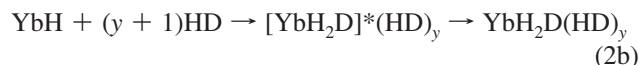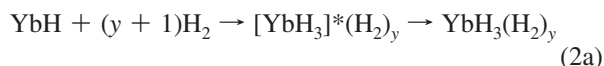| Tb | Dy | Ho | Er | Tm | Yb | Lu | ident$^b$ |
|---|---|---|---|---|---|---|---|
| | | | Pure Hydrogen | | | | |
| 3888 | 3884 | 3882 | 3888 | 3899 | 3902 | 3908 | 3 |
| [3755] | [3852] | [3747] | [3827] | [3848] | [3899] | [3936] | |
| 3309 | 3248 | 3151 | 3118 | n. o. | n. o. | n. o. | 2 |
| [3624] | [3760] | [3994] | [3911] | [4166] | [4191] | [3699] | |
| | | | 1461.9 | | 1206.6 | 1447.4 | 1, LnH |
| | | | [1208] | [1245] | [1226] | [1518] | |
| | | | {1424} | {1484} | {1336} | | |
| 1345.9 | 1360.2 | 1371.6 | 1377.3 | (1253.5) | (1251.6) | | 2 |
| [1375] | [1310] | [1270] | [1319] | [1294] | [1303] | [1522] | |
| 1330.1 | 1340.1 | 1348.9 | 1363.5 | 1381.3 | 1384.3 | 1393.3 | 3 |
| [1398] | [1414] | [1415] | [1437] | [1442] | [1448] | [1474] | |
| 1305.2 | 1318.6 | 1331.7 | 1338.8 | 1186.2 | 1184.5 | 1375.0 | 2 |
| [1343] | [1244] | [1224] | [1167] | [1241] | [1249] | [1465] | |
| 1212.0 | 1221.2 | 1231.8 | 1244.0 | 1226.4 | | 1278.7 | ? |
| 1212.0 | 1221.2 | 1231.8 | | | | | |
| 1110 | 1121 | 1144 | 1177 | 938 | 1101 | 1177 | 4$^-$ |
| [1206] | [1218] | [1244] | [1254] | [1135] | [1282] | [1267] | |
| 1092 | 1097 | 1104 | 1136 | 916 | 1063 | | 4$^-$ |
| [1206] | [1218] | [1244] | [1254] | [1135] | [1282] | | |
| | | | Deuterated Species | | | | |
| 2799.0 | 2795.1 | 2793.4 | 2795.5 | 2800.4 | 2801.7 | 2803.4 | 3 |
| 2749 | 2741 | 2734 | 2732 | | | | ? |
| 2692 | 2689 | 2684 | 2676 | | | | 2 |
| 2425 | 2389 | 2319 | 2297 | n. o. | n. o. | n. o. | 2 |
| | | | 1043.8 | | 866.4 | 1034.3 | 1, LnD |
| 961.4 | 971.1 | 977.5 | | | | | 2 |
| 951.2 | 957.9 | 964.1 | 974.6 | 985.5 | 990.7 | 993.6 | 3 |
| 935.9 | 945.0 | 952.3 | 961.1 | 880.4 | 844.1 | 983.5 | 2 |
| 851.4 | 870.9 | 884.5 | 893.2 | 900.4 | | 916.8 | ? |
| 803 | 830 | 821 | 830 | | | | 4$^-$ |
| 787.4 | 807.3 | 797.5 | 807.2 | | | | 4$^-$ |

$^a$ The most important calculated frequencies at the DFT/BPE0/TZVPP level of theory for the following molecules or super-complexes LnH, LnH$_2$(H$_2$), and LnH$_3$(H$_2$) are included in [brackets] or at the CASPT2 level of theory in {braces}. $^b$ Identification of absorption bands in the figures.

Three initial bands at 1388.7, 1207.9, and 1189.5 cm$^{-1}$, with increasing intensities, are 2−5 cm$^{-1}$ higher than the hydrogen matrix counterparts for YbH$_3$, YbH, and YbH$_2$, and these bands are assigned accordingly. The YbH$_2$ band increases more, and the YbH and YbH$_3$ species are more stable on UV irradiation in solid neon than in solid hydrogen: this implies that more Yb survives deposition to react with the limited (4%) H$_2$ on irradiation in solid neon than in solid hydrogen. These core molecules are probably almost as heavily ligated by H$_2$ as in solid hydrogen since the diffusion of H$_2$ in condensing neon is almost unlimited. However, the secondary neon solvent shell gives rise to a small blue shift. The ultimate yield of the YbH$_3$ species is, of course, higher in solid hydrogen than in solid neon.

Weak bands at 3309, 3248, 3151, and 3118 cm$^{-1}$ with Tb, Dy, Ho, and Er (Figure 1) decrease in intensity on irradiation and track in intensity with the Ln−H stretching modes assigned to species 2 (Figure 2), but counterparts were not observed for Tm, Yb, and Lu. These bands exhibit decreasing H/D isotopic frequency ratios from 1.364 to 1.357 cm$^{-1}$ from Tb to Er, which are in line for the H−H vibration of a hydrogen ligand with moderate bonding to the metal center and anharmonicity in the vibration for the corresponding LnH$_2$(H$_2$)$_y$ complexes.

Very weak bands from 3882 to 3908 cm$^{-1}$ (Figure 1, Table 1) increase on irradiation with the stronger trihydride Ln−H stretching absorptions, and they are assigned to the strongest H−H ligand vibration in the LnH$_3$(H$_2$)$_y$ complexes. The H/D isotopic frequency ratios increase from 1.389 to 1.394 from Tb to Lu, and these ratios are appropriate for H−H vibrations with little anharmonicity and weak binding to the metal center. For comparison the (H$^-$)(H$_2$)$_n$ complex H−H stretching absorption at 3972 cm$^{-1}$ in our Yb experiments is a consequence of a weak interaction, and little anharmonicity is evidenced by the 1.384 H/D isotopic frequency ratio.

The sharp doublet at 1206.6, 1204.7 cm$^{-1}$ for Yb in hydrogen disappears on >470 nm irradiation with the marked increase in YbH$_3$ (Figure 3). This photosensitive doublet shows a medium shift to 1209.3, 1206.7 cm$^{-1}$ in solid HD. In solid deuterium the band is at 866.4 cm$^{-1}$ (H/D ratio 1.393) and at 866.2 cm$^{-1}$ in solid HD. These bands are assigned to the YbH/YbD diatomic molecules where the minimum shifts between solid molecular hydrogens are attributed to weak ligand interactions. The visible photodestruction of YbH in solid hydrogen is then due to the straightforward reaction (2a). It is easy to visualize isotopic positional exchange for this reaction in solid HD. The sharp doublet observed here for YbH in solid hydrogen is hardly shifted from the gas phase 1207.3 cm$^{-1}$ nor is YbD significantly shifted from the 865.4 cm$^{-1}$ gas phase fundamental frequency,[21] which shows that the hydrogen ligand and matrix environment have little effect on the YbH molecule.

$$\text{YbH} + (y + 1)\text{H}_2 \rightarrow [\text{YbH}_3]^*(\text{H}_2)_y \rightarrow \text{YbH}_3(\text{H}_2)_y \quad (2a)$$

$$\text{YbH} + (y + 1)\text{HD} \rightarrow [\text{YbH}_2\text{D}]^*(\text{HD})_y \rightarrow \text{YbH}_2\text{D}(\text{HD})_y \quad (2b)$$

$$\text{YbH} + (y + 1)\text{HD} \rightarrow [\text{YbH}_2\text{D}]^*(\text{HD})_y \rightarrow \text{YbHD}_2(\text{H}_2)(\text{HD})_{y-1} \quad (2c)$$

The sharp doublet at 1226.4, 1224.1 cm$^{-1}$ in Tm experiments exhibits similar isotopic behavior: it shifts to 880.4, 878.1 cm$^{-1}$ in solid deuterium (H/D ratio 1.3930) and these bands are displaced only 2.3 and 0.4 cm$^{-1}$ in solid HD, which is

**TABLE 2: Spin Multiplicities for Each of the Electronic Ground-State Species Optimized at the DFT/PBE0/TZVPP Level of Theory[a]**

|  | Tb | Dy | Ho | Er | Tm | Yb | Lu |
|---|---|---|---|---|---|---|---|
| MH | Septet $6s^{1.6}4f^{8.0}5d^{0.2}$ | Sextet $6s^{1.6}4f^{9.0}5d^{0.2}$ | Quintet $6s^{1.2}4f^{10.9}5d^{0.1}$ | Quartet $6s^{1.2}4f^{12.0}5d^{0.1}$ | Triplet $6s^{1.2}4f^{13.0}5d^{0.1}$ | Doublet $6s^{1.2}4f^{14.0}5d^{0.1}$ | Singlet $6s^{1.9}4f^{14.0}5d^{0.2}$ |
| MH$_2$ | Sextet $6s^{1.1}4f^{8.0}5d^{0.3}$ | Quintet $6s^{1.1}4f^{9.0}5d^{0.3}$ | Quartet $6s^{0.5}4f^{10.9}5d^{0.2}$ | Triplet $6s^{0.7}4f^{11.7}5d^{0.2}$ | Doublet $6s^{0.5}4f^{13.0}5d^{0.1}$ | Singlet $6s^{0.5}4f^{14.0}5d^{0.1}$ | Doublet $6s^{1.1}4f^{14.0}5d^{0.4}$ |
| MH$_3$ | Septet $6s^{0.8}4f^{7.4}5d^{0.5}$ | Sextet $6s^{0.8}4f^{8.6}5d^{0.4}$ | Quintet $6s^{0.5}4f^{10.0}5d^{0.5}$ | Quartet $6s^{0.5}4f^{11.0}5d^{0.4}$ | Triplet $6s^{0.5}4f^{12.0}5d^{0.4}$ | Doublet $6s^{0.5}4f^{13.0}5d^{0.3}$ | Singlet $6s^{0.6}4f^{14.0}5d^{0.4}$ |
| MH$_4$ | Octet $6s^{0.9}4f^{7.0}5d^{0.6}$ | Septet $6s^{0.9}4f^{8.1}5d^{0.6}$ | Sextet $6s^{0.6}4f^{10.0}5d^{0.4}$ | Quintet $6s^{0.6}4f^{11.0}5d^{0.4}$ | Quartet $6s^{0.4}4f^{12.0}5d^{0.6}$ | Triplet $6s^{0.4}4f^{13.0}5d^{0.5}$ | Doublet $6s^{0.7}4f^{14.0}5d^{0.4}$ |
| MH$_2$(H$_2$) | Sextet $6s^{1.0}4f^{7.7}5d^{0.4}$ | Quintet $6s^{1.0}4f^{9.0}5d^{0.3}$ | Quartet $6s^{0.4}4f^{11.0}5d^{0.2}$ | Triplet $6s^{0.6}4f^{11.6}5d^{0.2}$ | Doublet $6s^{0.4}4f^{13.0}5d^{0.1}$ | Singlet $6s^{0.4}4f^{14.0}5d^{0.1}$ | Doublet $6s^{1.0}4f^{14.0}5d^{0.4}$ |
| MH$_3$(H$_2$) | Septet $6s^{0.8}4f^{7.4}5d^{0.5}$ | Sextet $6s^{0.8}4f^{8.6}5d^{0.4}$ | Quintet $6s^{0.4}4f^{10.0}5d^{0.4}$ | Quartet $6s^{0.4}4f^{11.0}5d^{0.4}$ | Triplet $6s^{0.4}4f^{12.0}5d^{0.4}$ | Doublet $6s^{0.4}4f^{13.0}5d^{0.3}$ | Singlet $6s^{0.5}4f^{14.0}5d^{0.4}$ |

[a] The main contribution to the natural electronic configuration of each metal has also been given.

appropriate for a TmH assignment. This band is destroyed by >470 nm irradiation while the strong 3 band increases 3-fold (spectrum identical to that of Figure 1j). The above-described agreement for our YbH band and the gas phase spectrum further suggests that the gas phase observation of TmH will be near our hydrogen matrix observation. However with Lu, the band that gives way on >470 nm irradiation to LuH$_3$ is now higher at 1447.4 cm$^{-1}$, which shifts to 1034.3 cm$^{-1}$ in deuterium (H/D ratio 1.3994). The gas phase spectrum[33] reveals an approximate anharmonic frequency of 1476 ± 20 cm$^{-1}$, which supports this assignment to the LuH core molecule.

It thus appears that there are two regions for Ln−H frequencies, low 1200 cm$^{-1}$ and mid 1400 cm$^{-1}$ depending on the 4f orbital core configuration. The Er spectrum has two sharp bands that are candidates for the ErH absorption, at 1461.9 and at 1244.0 cm$^{-1}$. The former is destroyed on >470 nm irradiation which doubles the ErH$_3$ absorption while the latter increases 20%. These bands exhibit deuterium counterparts at 1043.8 and 893.2 cm$^{-1}$ and H/D ratios 1.4006 and 1.3927 and are shifted less than 2 cm$^{-1}$ in solid HD. Both are appropriate for ErH/ ErD core absorptions as far as experimental isotopic shifts are concerned. We are inclined, on the basis of the behavior on >470 nm irradiation and the CASSCF/CASPT2 prediction of a 1427 cm$^{-1}$ fundamental, to assign the 1461.9 cm$^{-1}$ band to the ErH core molecule in solid hydrogen. The assignment of this peak is at the basis of a controversy that we found in our calculations. Both the DFT/BP86/TZVPP and DFT/PBE0/ TZVPP methods give a ground state for ErH with an electronic valence configuration of $6s^{1}4f^{12}$ for the erbium atom and a stretching mode of 1194 cm$^{-1}$ (BP86). The CASSCF/CASPT2 method, on the other hand, predicts a different ground state, with a valence configuration of $6s^{1}5d^{1}4f$,[11] where one electron is promoted from the 4f to the 5d shell. This electronic state is much higher in energy at the DFT level and the state predicted as the ground state at the CASPT2 level did not come up as a low lying state at the DFT level of theory. Even if the two methods predict different ground states, they predict quite similar stretching modes, namely, 1395 cm$^{-1}$ (DFT/BP86) and 1427 cm$^{-1}$ (CASSCF/CASPT2). The two levels of theory predict a different electronic ground state most likely because of the highly multiconfigurational nature of the ground state wave function, which can be accurately described only by the CASSCF/CASPT2 approach. However, the experimental evidence of two bands suggests the occurrence of close-lying states that can be trapped at the same time in the matrix at different experimental irradiations.

A similar pattern has been found for the TmH fundamental, computed at 1484 cm$^{-1}$ at the CASSCF/CASPT2 level of theory, with a valence configuration of the Tm atom of $6s^{1}5d^{1}4f$,[12] and at 1196 cm$^{-1}$ at the BP86 level of theory, with a Tm configuration of $6s^{1}4f^{13}$. This lower value is more in line with the sharp doublet measure at 1226.4, 1224.1 cm$^{-1}$ in the Tm experiments.

For Tb, Dy, and Ho we observed sharp, weak 1212.0, 1221.2, and 1231.8 cm$^{-1}$ bands in the lower region where LnH absorptions might be observed. These bands increase slightly on sample irradiation. Appropriate deuterium shifted values are observed for LnH(D) stretching modes (Table 1), but the yield is too low for observation of HD counterparts, so these bands are for now not assigned.

**Calculations**

Density functional and CASSCF/CASPT2 calculations were performed for the late lanthanide metal core hydrides and several dihydrogen complexes. The computed vibrational frequencies, reported in Table 1, were discussed previously together with the experimental ones. The remaining computational results are reported in Tables 2−4 including the electronic ground states of the products (Table 2).

Several trends are apparent. First, the binding of H$_2$ ligands to late LnH$_x$ core molecules is weak in general, and the number of ligands (*y*) is small, 1 or 2 (Tables 3 and 4). Inspection of Table 3 shows that the trihydrides bind more strongly than the dihydrides. This trend is opposite compared to the trend found for the early lanthanides.[16] Moreover the binding decreases going across the row, which could be a reflection of the lanthanide contraction. These conclusions are mainly qualitative, in the sense that the interaction energies that we are comparing are small and almost of the same order of magnitude of the error associated with the DFT method.

Another qualitative conclusion can be drawn by looking at the H−H stretching frequencies of the H$_2$ molecule, peripherally attached to the metal di- and trihydrides. Experimentally this mode falls at a much lower frequency when the molecule is attached to the LnH$_2$ as compared to the LnH$_3$. Intuitively, this can be associated with a weaker bond between the two molecular units, confirming what was said in the previous paragraph. However, the origin of such a frequency shift is based mostly on a different charge transfer from the LnH$_x$ core unit to the H$_2$ molecule. In Table 5, an analysis of the natural charges indicates that for TbH$_2$ and DyH$_2$, the charge migration to the antibonding molecular orbital of the H$_2$ molecule is about twice as large as that from TbH$_3$ and DyH$_3$. As an effect, the strength of the HH bond decreases and consequently the stretching mode frequency is reduced. This fact does not automatically imply that the bond

**TABLE 3: Stabilization Energy (kcal/mol) of the Supercomplex MH$_x$(H$_2$)$_y$ upon Adding H$_2$ Molecules on the Simple MH$_n$ Monomer, Computed Using the DFT/BP86/TZVPP Level of Theory[a]**

| | Tb | Dy | Ho | Er | Tm | Yb | Lu |
|---|---|---|---|---|---|---|---|
| **MH$_2$** | | | | | | | |
| 1 H$_2$ | −4.2 | −3.7 | −2.9 | 0.1 | −1.0 | −1.2 | −2.3 |
| | (−0.8) | (−0.5) | (−0.3) | (2.7) | (1.3) | (0.9) | (0.9) |
| | {−6.6} | {−3.7} | {−5.3} | {−1.3} | {−2.3} | {−2.2} | {−2.6} |
| | {(−3.0)} | {(−0.5)} | {(−2.3)} | {(1.3)} | {(−0.2)} | {(−0.1)} | {(0.7)} |
| 2 H$_2$ | −9.7 | −7.5 | −4.2 | −0.8 | −2.2 | −2.8 | −3.1 |
| | (−3.3) | (−1.6) | (1.0) | (4.3) | (2.1) | (1.7) | (2.9) |
| | {−8.2} | {−10.2} | {−6.9} | {−2.0} | {−4.3} | {−4.5} | {−3.8} |
| | {(−1.9)} | {(−4.1)} | {(−2.2)} | {(4.8)} | {(0.2)} | {(0.0)} | {(2.5)} |
| **MH$_3$** | | | | | | | |
| 1 H$_2$ | −4.9 | −1.0 | −5.2 | −6.8 | −2.6 | −3.4 | −3.7 |
| | (−0.8) | (0.8) | (−1.6) | (−2.9) | (1.2) | (−0.3) | (−0.1) |
| | {−7.3} | {−3.4} | {−5.2} | {−6.2} | {−5.7} | {−5.2} | {−4.4} |
| | {(−3.8)} | {(0.0)} | {(−1.5)} | {(−2.3)} | {(−2.0)} | {(−1.4)} | {(−0.9)} |
| 2 H$_2$ | −8.6 | | −8.7 | −10.1 | −6.4 | −5.6 | −7.6 |
| | (−1.1) | | (−1.9) | (−2.7) | (0.2) | (0.1) | (−0.7) |
| | {−12.4} | {−3.6} | {−12.2} | {−11.3} | {−10.9} | {−9.6} | {−9.0} |
| | {(−5.4)} | {(−4.4)} | {(−5.1)} | {(−3.9)} | {(−3.7)} | {(0.0)} | {()} |

[a] A negative energy means that the supercomplex is more stable than its fragments. In (parentheses), we include the ZPE. In {braces}, the DFT/PBE0/TZVPP energies are presented.

**TABLE 4: Stabilization Energy (kcal/mol) of the Supercomplexes MH$_3$ and MH$_4$ upon Adding One H or One H$_2$ to the MH$_2$ or MH$_3$ Units, Computed Using the DFT/PBE0/TZVPP Level of Theory[a]**

| | Tb | Dy | Ho | Er | Tm | Yb | Lu |
|---|---|---|---|---|---|---|---|
| MH$_3$ + H → MH$_4$ | −32.0 | −22.3 | −17.0 | −16.5 | −34.6 | −32.4 | −16.8 |
| | (−29.3) | (−20.5) | (−15.4) | (−14.6) | (−29.8) | (−39.1) | (−15.5) |
| | {−17.9} | {−1.2} | {−5.9} | {−3.0} | {−34.1} | {−30.8} | {} |
| | {(−14.7)} | {(2.8)} | {(−5.2)} | {(−2.0)} | {(−29.2)} | {(−25.8)} | {()} |
| MH$_3$ + H$^-$ → MH$^-_4$ | −87.4 | −77.1 | −92.3 | −89.6 | −87.2 | −83.8 | −96.1 |
| | (−84.9) | (−74.6) | (−89.4) | (−86.6) | (−84.4) | (−80.9) | (−93.5) |
| | {−95.5} | {−84.1} | {−97.6} | {−94.6} | {−97.1} | {−96.5} | {−97.9} |
| | {(−93.5)} | {(−81.5)} | {(−95.2)} | {(−92.0)} | {(−94.5)} | {(−93.7)} | {(−95.0)} |
| MH$_2$ + H$_2$ → MH$_4$ | 21.0 | 39.4 | 48.4 | 47.4 | 37.4 | 47.1 | 23.2 |
| | (27.1) | (44.7) | (53.5) | (52.3) | (45.1) | 36.6 | (28.1) |
| | {13.2} | {40.1} | {36.4} | {35.5} | {26.5} | {46.3} | {29.9} |
| | {(20.8)} | {(48.1)} | {(41.5)} | {(40.9)} | {(29.4)} | {(49.2)} | {(27.9)} |
| MH + H$_2$ → MH$_3$ | −6.4 | 4.1 | 9.5 | 5.4 | 14.7 | 21.4 | −19.4 |
| | (−6.9) | (3.6) | (9.2) | (4.9) | (14.0) | (20.2) | (−19.2) |
| | {−25.9} | {−11.7} | {−11.3} | {−15.6} | {5.1} | {21.9} | {−22.6} |
| | {(−25.4)} | {(−11.8)} | {(−10.8)} | {(−15.2)} | {(5.5)} | {(22.2)} | {(−20.5)} |

[a] A negative energy means that the MH$_4$ (or MH$_3$) complex is more stable than its fragments. In (parentheses), we include the ZPE. In {braces}, the DFT/PBE0/TZVPP energies are also reported.

**TABLE 5: Natural Population Analysis at DFT/PBE0/TZVPP Level of Theory for the Dihydride and Three-Hydride Systems with One H$_2$ Molecule[a]**

| | Tb | Dy | Ho | Er | Tm | Yb | Lu |
|---|---|---|---|---|---|---|---|
| MH$_2$ | 0.16 | 0.12 | 0.05 | 0.06 | 0.02 | 0.02 | 0.12 |
| MH$_3$ | 0.08 | 0.07 | 0.07 | 0.06 | 0.06 | 0.04 | 0.04 |

[a] The numbers indicate the amount of electronic charge transferred from the metal to the H$_2$ unit.

between LnH$_2$ and H$_2$ is stronger, because other factors can play a role, such as the electrostatic interaction (for example, the partial positive charge on the lanthanide atom in LnH$_3$ is larger than that in LnH$_2$, with a possible increase of the charge-induced dipole interaction term for the trihydride) and the Pauli repulsion (more contracted lanthanide atom, thus less repulsion between LnH$_3$ and H$_2$). In Table 5, we further notice that, while the charge transfer is similar in the whole LnH$_3$ series, for the LnH$_2$ series, a step occurs from Dy to Ho and the rest of the series, with the exception of Lu. This is most likely due to the low-lying states of the LnH$_2$ molecule that can easily change order once the fragment interacts with the molecular hydrogen. In

our DFT calculations of the supercomplexes we always searched for the lowest solution without any symmetry constraint. This explains the possibility of a different charge transfer pattern along the series. Moreover, the lack of noticeable bands in the experiment for the latest LnH$_2$ may be caused by this change in the electronic state.

Second, the isolated LnH$_3$ molecules are calculated to be planar with no symmetry and three different Ln−H stretching frequencies: for example, TbH$_3$ has two degenerate modes at 1385 cm$^{-1}$ and one weak one at 1630 cm$^{-1}$ (See Supporting Information.) As 1 and 2 H$_2$ ligands are attached, the degenerate mode splits in two peaks, at slightly higher and lower frequencies than the bare TbH$_3$, while the weak mode is red-shifted to 1462 cm$^{-1}$ and is more intense. The ligand modes increase from 3755 cm$^{-1}$ for a single dihydrogen ligand to 3842 and 3878 cm$^{-1}$ for two ligands. This models our observation of a single strong 1330 cm$^{-1}$ Tb−H stretching mode (Tb−D counterpart at 951 cm$^{-1}$, H/D frequency ratio 1.398) and weak (low infrared intensity) H−H stretching frequency at 3888 cm$^{-1}$ (D−D counterpart at 2799 cm$^{-1}$, H/D ratio 1.389) reasonably well. Remember that the TbH$_3$(H$_2$)$_y$ complex is embedded in a

secondary shell of $z$ H$_2$ molecules, i.e., the solid hydrogen matrix cage, and the weak 3888 cm$^{-1}$ band in the spectrum could be due to such H–H vibrations instead of the $y$ H$_2$ ligands.

Third, the isolated LnH$_2$ molecules are calculated to be bent, and the symmetric Ln–H stretching mode is observed for the first four of the late lanthanides above the strong band that is assigned to the MH$_3$ species. Weak bands are observed at 1254 and 1252 cm$^{-1}$, which are probably due to the symmetric stretching modes of the TmH$_2$ and YbH$_2$ core molecules.

Fourth, the diatomic molecules LnH have also been calculated, which may be compared to earlier results.[4–6] We have also computed the energetics of the basic (reaction 2a) without ligands and find them to be exothermic (Table 3). Hence, the above 1226 cm$^{-1}$ band, which compares favorably to our 1204 cm$^{-1}$ harmonic fundamental for the doublet ground state of YbH, behaves appropriately for YbH, and it is so assigned. The gas phase fundamental frequency is 1207.3 cm$^{-1}$, which shows that the hydrogen matrix causes little shift in the vibrational fundamental.[32] Likewise, the 1447.4 cm$^{-1}$ band with Lu is destroyed on vis irradiation which produces LuH$_3$, and it is appropriate for singlet ground state LuH, which is near the 1476 $\pm$ 20 cm$^{-1}$ gas phase fundamental and in the range of our 1518 cm$^{-1}$ and other 1470–1440 cm$^{-1}$ DFT and the 1507 cm$^{-1}$ CCSD(T) computed values.

Finally, in Table 5 the natural population analysis is reported, as already mentioned previously. The amount of charge transferred from the metal to the H$_2$ unit decreases along the lanthanide series, and more charge transfer occurs in the MH$_2$ species than the MH$_3$ species.

## Conclusions

A combined experimental and theoretical investigation of late lanthanide metal atom reaction products with pure hydrogen during condensation at 4 K is reported. As found for the early lanthanide metals reacting with pure hydrogen, the dominant product is the metal trihydride with absorptions in the 1330–1400 cm$^{-1}$ region and very weak ligand bands near 3900 cm$^{-1}$, based on deuterium substitution and density functional theory frequency calculations. With ytterbium, YbH and YbH$_2$ were the major initial products, but YbH$_3$ increased at their expense upon sample irradiation. Evidence is also presented for the LuH and ErH molecules and the tetrahydride anions in solid hydrogen.

Dihydrogen complex formation is weaker with the late lanthanide metal hydrides than with their early lanthanide counterparts, which is probably a consequence of lanthanide contraction.

**Supporting Information Available:** Calculated frequencies and geometrical coordinates for all structures and infrared spectra for the late lanthanide reactions with hydrogen and deuterium. This material is available free of charge via the Internet at http://pubs.acs.org.

## References and Notes

(1) Cotton, F. A.; Wilkinson, G.; Murillo, C. A.; Bochmann, M. *Advanced Inorganic Chemsitry*, 6th ed.; Wiley: New York, 1999.
(2) Ruspic, C.; Spielmann, J.; Harder, S. *Inorg. Chem.* **2007**, *46*, 5320–5326.
(3) Dolg, M.; Stoll, H. *Theor. Chim. Acta* **1989**, *75*, 369–387.
(4) Liu, W. J.; Dolg, M.; Li, L. M. *J. Chem. Phys.* **1998**, *108*, 2886–2895.
(5) Cao, X. Y.; Dolg, M. *J. Chem. Phys.* **2001**, *115*, 7348–7355.
(6) Jalbout, A. F.; Li, X. H.; Abou-Rachid, H. *Int. J. Quantum Chem.* **2007**, *107*, 522–539.
(7) Maron, L.; Eisenstein, O. *J. Phys. Chem. A* **2000**, *104*, 7140–7143.
(8) Luo, Y.; Hou, Z. M. *J. Phys. Chem. C* **2008**, *112*, 635–638.
(9) Bauhofer, W.; Joss, W.; Kremer, R. K.; Mattausch, H.; Simon, A. In *International Conference on Magnetism*; Elsevier Science Bv: Edinburgh, Scotland, 1991; pp 1243–1244.
(10) Vajda, P.; Daou, J. N. *Phys. Rev. B* **1994**, *49*, 3275–3282.
(11) Huiberts, J. N.; Griessen, R.; Rector, J. H.; Wijnaarden, R. J.; Dekker, J. P.; deGroot, D. G.; Koeman, N. J. *Nature* **1996**, *380*, 231–234.
(12) Andrews, L. *Chem. Soc. Rev.* **2004**, *33*, 123–132.
(13) Wang, X. F.; Andrews, L.; Infante, I.; Gagliardi, L. *J. Am. Chem. Soc.* **2008**, *130*, 1972–1978.
(14) Wang, X. F.; Andrews, L. *Organometallics* **2008**, *27*, 4273–4276.
(15) Raab, J.; Lindh, R. H.; Wang, X. F.; Andrews, L.; Gagliardi, L. *J. Phys. Chem. A* **2007**, *111*, 6383–6387.
(16) Infante, I.; Gagliardi, L.; Wang, X. F.; Andrews, L. *J. Phys. Chem. A* **2009**, *113*, 2446–2455.
(17) Willson, S. P.; Andrews, L. *J. Phys. Chem. A* **2000**, *104*, 1640–1647.
(18) Andrews, L.; Citra, A. *Chem. Rev.* **2002**, *102*, 885–911.
(19) Ahlrichs, R.; Bar, M.; Haser, M.; Horn, H.; Kolmel, C. *Chem. Phys. Lett.* **1989**, *162*, 165–169.
(20) Roos, B. O.; Taylor, P. R.; Siegbahn, P. E. M. *Chem. Phys.* **1980**, *48*, 157–173.
(21) Andersson, K.; Malmqvist, P.-Å.; Roos, B. O. *J. Chem. Phys.* **1992**, *96*, 1218–1226.
(22) Hess, B. A. *Phys. Rev. A* **1986**, *33*, 3742–3748.
(23) Karlström, G.; Lindh, R.; Malmqvist, P.-Å.; Roos, B. O.; Ryde, U.; Veryazov, V.; Widmark, P.-O.; Cossi, M.; Schimmelpfennig, B.; Neogrady, P.; Seijo, L. *Comput. Mater. Sci.* **2003**, *287*, 222–239.
(24) Gagliardi, L. *J. Am. Chem. Soc.* **2003**, *125*, 7504–7505.
(25) Gagliardi, L.; Roos, B. O. *Nature* **2005**, *433*, 848–851.
(26) Gagliardi, L.; Roos, B. O. *Chem. Soc. Rev.* **2007**, *36*, 893–903.
(27) Gagliardi, L.; Pyykko, P. *Angew. Chem., Int. Ed.* **2004**, *43*, 1573–1576.
(28) Gagliardi, L.; La Manna, G.; Roos, B. O. *Faraday Discuss.* **2003**, *124*, 63–68.
(29) Gagliardi, L.; Pyykko, P.; Roos, B. O. *Phys. Chem. Chem. Phys.* **2005**, *7*, 2415–2417.
(30) Roos, B. O.; Gagliardi, L. *Inorg. Chem.* **2006**, *45*, 803–807.
(31) Wang, X. F.; Andrews, L. *J. Phys. Chem. A* **2004**, *108*, 1103–1106.
(32) Wang, X. F.; Andrews, L. *J. Phys. Chem. A* **2002**, *106*, 3706–3713.
(33) Huber, K. P.; Herzberg, G. *Constants of Diatomic Molecules*; Van Nostrand Reinhold: New York, 1979.
(34) Cao, X. Y.; Moritz, A.; Dolg, M. *Chem. Phys.* **2008**, *343*, 250–257.